Advances in Nano Research, *Vol. 17, No.4 (2024) 335-350*
https://doi.org/10.12989/anr.2024.17.4.335

Refined nonlocal strain gradient theory for mechanical response of cosine FG-GRNC laminated nanoshells rested on elastic foundation

Mohamed A. Eltaher*[1], A.A. Daikh[2,3], Amin Hamdi[4], Gamal S. Abdelhaffez[5] and Azza M. Abdraboh[6]

[1]*Mechanical Engineering Department, Faculty of Engineering, King Abdulaziz University, P.O. Box 80204, Jeddah, Saudi Arabia*
[2]*Department of Technical Sciences, Center University Salhi Ahmed, Naâma 45000, Algeria*
[3]*Laboratoire d'Etude des Structures et de Mécanique des Matériaux, Département de Génie Civil, Faculté des Sciences et de la Technologie, Université Mustapha Stambouli, Mascara, Algerie*
[4]*Civil and Environmental Engineering Department, King Abdulaziz University, Jeddah, Saudi Arabia*
[5]*Department of Mining Engineering, Faculty of Engineering, King Abdulaziz University, Jeddah, Saudi Arabia*
[6]*Physics Department, Faculty of Science, Benha University, Benha, Egypt*

(*Received August 11, 2021, Revised September 24, 2024, Accepted October 2, 2024*)

Abstract. This paper investigates the mechanical behavior of a new type of functionally graded graphene-reinforced nanocomposite (FG-GRNC) doubly-curved laminated shells, referred to as cosine FG-GRNC. The study employs a refined higher-order shear deformation shell theory combined with a modified continuum nonlocal strain gradient theory. The effective Young's modulus of the GRNC shell in the thickness direction is determined using the modified Halpin-Tsai model, while Poisson's ratio and mass density are calculated using the rule of mixtures. The analysis includes two graphene-reinforced distribution patterns—FG-A CNRCs and FG-B CNRCs—along with uniform UD CNRCs. An enhanced Galerkin method is used to solve the governing equilibrium equations for the GRNC nanoshell, yielding closed-form solutions for bending deflection and critical buckling loads. The nanoshell is supported by an orthotropic elastic foundation characterized by three parameters. A detailed parametric analysis is performed to evaluate how factors such as the length scale parameter, nonlocal parameter, distribution pattern, GPL weight fraction, shell thickness, and shell geometry influence deflections and critical buckling loads.

Keywords: cosine FG-CNTRC shells; galerkin method; higher-order shear deformation theory; mechanical response; refined displacement field; orthotropic elastic foundation

1. Introduction

Over the past decades, the striving for lighter and stronger structures has resulted in an increasing use of advanced materials (Stegmann and Lund 2005). Functionally Graded Materials (FGMs) represent a significant advancement in materials science, characterized by a gradual variation in composition and structure over their volume, which optimizes material properties to meet specific engineering demands (Belarbi *et al*. 2023, Daikh *et al*. 2018, Alazwari *et al*. 2021, Tharwan *et al*. 2024). This gradient enhances performance in high-performance contexts such as aerospace, civil engineering, and electronics by providing superior thermal resistance, mechanical strength, and tailored properties. Building on this concept, Functionally Graded Distribution Graphene-Reinforced Nanocomposites (FG-GRNCs) offer even more significant advancements by incorporating graphene reinforcement into FGMs. FG-GRNCs further enhance strength-to-weight ratios, durability, and overall performance, making them particularly valuable in aerospace, civil, and automotive industries. Additionally, their potential application in smart materials for real-time structural health monitoring underscores their broad and impactful practical uses. Composite shell panel structures are used extremely in aerospace structures (i.e., fuselages, tanks, radomes, wing skins), chemical, mechanical, and other engineering applications, because of their excellent mechanical performance with outstanding mechanical properties such as lightweight, high specific stiffnesses, high specific strengths and durability (Abo-bakr *et al*. 2024).

Shen and Zhang (2010) investigated the thermal buckling/ postbuckling behavior for supported functionally graded carbon nanotubes-reinforced composite (FG-CNTRC) plates subjected to in-plane temperature variation. For shell structures, Shen (2011) studied the postbuckling of FG-CNTRC cylindrical shells in thermal environments under axial loads and pressure loads based on a higher order shear deformation theory with a von Kármán-type of kinematic nonlinearity by using the singular perturbation technique. Mercan *et al*. (2016) exploited the discrete singular convolution technique in analysing the vibration response of FG cylindrical shells with power-law index. Hasrati *et al*. (2017) used a numerical strategy to study nonlinear forced vibration analysis of FG-CNTRC cylindrical shells under thermal loading. Thang *et al*. (2019) derived the closed-form solution for nonlinear buckling analysis of FG-CNTRC cylindrical shells with initial geometric imperfections. Shen *et al*. (2020) studied the large

*Corresponding author, Professor,
E-mail: meltaher@kau.edu.sa

Copyright © 2024 Techno-Press, Ltd.

ISSN: 2287-237X (Print), 2287-2388 (Online)

amplitude vibration of FG-CNTRC laminated cylindrical shells with negative Poisson's ratio. Akbas *et al*. (2021) presented the dynamic responses of a fiber-reinforced composite beam under a moving load. The Timoshenko beam theory was employed to analyze the kinematics of the composite beam. Melaibari *et al*. (2022a, b) examined a dynamic response of randomly oriented functionally graded carbon nanotubes/fiber-reinforced composite laminated shells, with different geometries by using the Galerkin approach. Sun *et al*. (2022) presented the nonlinear vibration analysis of FG-CNTRC cylindrical shells resting on elastic foundations According to the first-order shear deformation shell theory. Shen *et al*. (2023) examined the postbuckling behaviors of pressure-loaded laminated cylindrical FG-CNTRC shells under thermal environmental conditions. Ninh *et al*. (2023) investigated dynamical characteristics of complex-generatrix cylindrical shells (CGCS) made of advanced composite with profiles defined by mathematical functions. Vu *et al*. (2023) developed a new analytical approach for nonlinear buckling and postbuckling of torsion-loaded FG-CNTRC sandwich toroidal shell segments with corrugated cores in thermal environments. Phon *et al*. (2024) illustrated the thermoelastic analysis of FG-CNTRC cylindrical shells with various boundary conditions and temperature-dependent characteristics using quasi-3D higher-order shear deformation theory. Zhao *et al*. (2024) exploited using generalized differential quadrature method in studying the thermal buckling of temperature-dependent FG-CNTRC conical-conical joined shell. Li and She (2024) studied nonlinear transient response analysis of rotating carbon nanotube reinforced composite cylindrical shells with initial geometrical imperfection.

Using modified nanoscale continuum theories, Bouadi *et al*. (2018) and Safaei *et al*. (2019) examined the buckling behavior of single-layered graphene sheets by utilizing the NLSG theory. Jalaei and Civalek (2019) investigated the dynamic instability of viscoelastic porous functionally graded (FG) nanobeam embedded on visco-Pasternak medium subjected to an axially oscillating loading as well as a magnetic field. The vibrational behavior of nano-single-layer graphene sheet has been investigated by Ghannadpour Moradi (2019), Mehrez *et al*. (2020) and Shariati *et al*. (2020). Dastjerdi *et al*. (2020) presented the size- and time-dependent viscoelastic bending analysis of rotating spherical nanostructures made of functionally graded materials under gyroscopic rotation. Esen *et al*. (2021) examined the dynamic response of nonlocal strain gradient FG nanobeam reinforced by carbon nanotubes under moving point load. Esmaeilzadeh *et al*. (2021) studied the thermo-mechanical comportment of the graphene-reinforced moving polymer nanoplates. Qu *et al*. (2021) examined bending and symmetric-shear deformations of a microstructure-dependent FG-MEE composite beam under mechanically induced electric and magnetic fields. Civalek and Avcar (2022) studied free vibration and buckling response of functionally graded carbon nanotube-reinforced laminated plates, using a four-nodded straight-sided transformation method. Alazwari *et al*. (2022) explored the dynamic behavior of temperature-dependent Reddy FG nanobeam subjected to thermomagnetic effects under the action of moving point load. Daikh *et al*. (2022) examined the static and dynamic stability responses of multilayer FG-CNTRC nanoplates via quasi 3D nonlocal strain gradient theory. Daikh *et al*. (2023) studied the buckling of bi-coated FG porous nanoplates via a nonlocal strain gradient quasi-3D theory. Wang *et al*. (2023) studied bending and wave propagation behaviors of axially functionally graded beams based on a reformulated strain gradient elasticity theory. Wang *et al*. (2024) developed an accurate numerical method for the static and dynamic response analysis of magneto-electro-elastic functionally graded microplates with complex geometries. Guerroudj *et al*. (2024) studied the free vibration behavior of FG nanobeam is presented in this work using the recently proposed nonlocal higher-order shear deformation theory. Ghazwani *et al*. (2024) presented the role of nonlocality on low and high-frequency behaviors and modes of FG sandwich nanoplates using simple nonlocal higher-order shear deformation theory. Uzun and Yaylı (2024) developed accurate and efficient analytical simulation of free vibration for embedded nonlocal CNTRC beams with general boundary conditions. Saffari *et al*. (2024) presented the effect of a magnetic field on the vibration of electro-rheological fluid nanoplates with FG-CNTRC layers. Zhang and Lu (2024) studied the non-linear free and forced vibration of bi-directional functionally graded truncated conical tubes based on the nonlocal gradient strain theory.

This research represents the first examination of the bending and buckling behaviours of cosine functionally graded graphene-reinforced nanocomposite (FG-GRNC) laminated nanoshells, significantly contributing to the scientific literature. The proposed nanocomposite shell rests on an orthotropic elastic foundation, chosen for its capability to accurately capture directional variations in stiffness, which significantly enhances the precision of deflection and buckling load predictions in engineering applications. The analysis employs a refined Galerkin approach that simplifies the problem by reducing the number of displacement variables. This solution is specifically tailored to cases with uniform thicknesses and symmetric boundary conditions (e.g., SSSS, CCCC, CCSS). The study includes a comprehensive comparative analysis and numerical simulations that detail the buckling and bending responses of cosine FG-GRNC laminated nano-shells supported by a complex elastic foundation. The results are thoroughly discussed in the results section.

2. Material properties of the FG-GRNC shell

Consider an FG-GRNC shell characterized by its geometric properties: length a, width b, thickness h, and radii R_x and R_y as depicted in Fig. 1. This shell is composed of an isotropic polymer matrix reinforced with graphene nanoplatelets (GPLs). The distribution of GPLs varies continuously across the thickness of the shell. Alongside a uniform GPL distribution pattern (UD-GRNC), two alternative GPL distribution patterns based on trigonometric functions are examined: FG-A-GRNC and FG-B-GRNC.

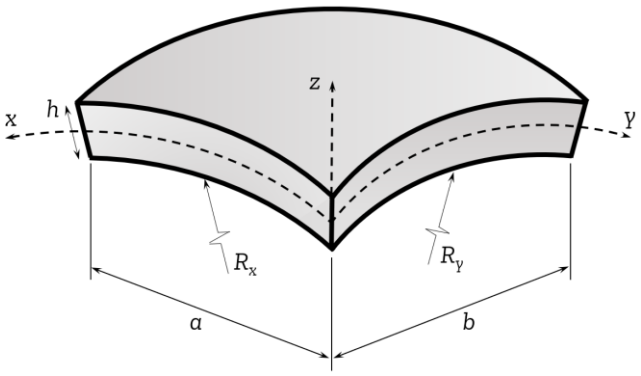

Fig. 1 Geometry of FG-GRC laminated shell

For FG-A-GRNC shells, the GPL weight fraction is zero at both the top and bottom surfaces, with the maximum concentration located at the centre of the nanoshell. Conversely, FG-B-GRNC shells feature an opposite GPL weight distribution compared to FG-A-GRNC shells, with the maximum GPL concentration at the top and bottom surfaces and minimal GPLs at the centre. The weight fraction patterns of the GPLs are described as follows:

$$\begin{aligned} &\text{UD:} \quad g_{GPL} = g^*_{GPL} \\ &\text{FG}-\text{A:} \quad g_{GPL} = g^*_{GPL}\left[1+\cos\left(N\frac{2\pi z}{h}\right)\right] \\ &\text{FG}-\text{B:} \quad g_{GPL} = g^*_{GPL}\left[1-\cos\left(N\frac{2\pi z}{h}\right)\right] \end{aligned} \tag{1}$$

where "N" represents the material inhomogeneity parameter (see Fig. 1), and g^*_{GPL} denotes the total weight fraction of GPLs. For even values of "N", the function defining the FG pattern transitions from FG-A to FG-B, meaning FG-A will become FG-B and FG-B will become FG-A.

Using the Halpin–Tsai model, the effective Young's modulus of the shell can be expressed as follows, based on the work of Affdl and Kardos (1976):

$$E = \frac{3}{8}\frac{1+\xi_L\eta_L V_{GPL}}{1-\eta_L V_{GPL}}E_m + \frac{5}{8}\frac{1+\xi_W\eta_W V_{GPL}}{1-\eta_W V_{GPL}}E_m \tag{2}$$

V_{GPL} is the GPLs volume fraction, where:

$$V_{GPL} = \frac{g_{GPL}}{g_{GPL} + (\rho_{GPL}/\rho_m)\left(1-g^{(k)}_{GPL}\right)} \tag{3}$$

and

$$\eta_L = \frac{(E_{GPL}/E_m)-1}{(E_{GPL}/E_m)+\xi_L} \tag{4}$$

$$\eta_W = \frac{(E_{GPL}/E_m)-1}{(E_{GPL}/E_m)+\xi_W} \tag{5}$$

$$\xi_L = 2\left(\frac{a_{GPL}}{h_{GPL}}\right) \tag{6}$$

$$\xi_W = 2\left(\frac{w_{GPL}}{h_{GPL}}\right) \tag{7}$$

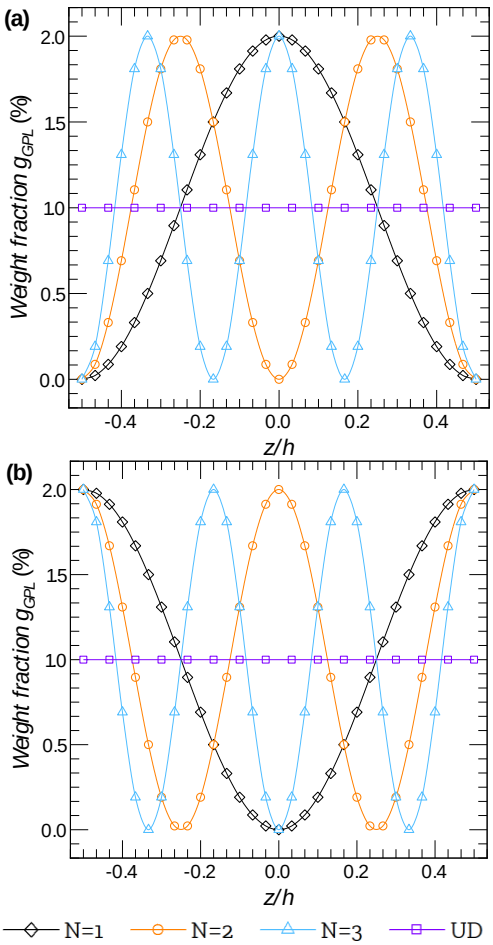

Fig. 2 Distribution of g_{GPL} through the shell thickness direction (a) FG-A, (b) FG-B

The effective mass density and the Poisson's ratio ρ and υ of the shell are calculated using the rule of mixtures, with their expressions given as follows:

$$\upsilon = \upsilon_{GPL}V_{GPL} + \upsilon_m V_m \tag{8}$$

$$\rho = \rho_{GPL}V_{GPL} + \rho_m V_m \tag{9}$$

Here, V_m presents the matrix $(V_m = 1 - V_{GPL})$. υ_{GPL} and υ_m are Poisson's ratio of the GPLs reinforcement and the epoxy matrix, respectively.

3. Displacement field

To characterize the displacement field, a novel hyperbolic shear theory is introduced. The proposed displacement field relies on several fundamental assumptions: the shell is of uniform thickness h h, and its material properties exhibit symmetry relative to the mid-plane. Moreover, the boundary conditions on opposing edges of the shell are uniform (e.g., SSSS, CCCC, CCSS), and any externally applied transverse loads are symmetric, including sinusoidal or uniform distributions. The above assumptions were proposed to ensure the same rotations in x and y directions. Considering the above assumptions, the displacement field can be written as follows:

$$u(x,y,z)=\left(1+\frac{z}{R_x}\right)u_0(x,y)-z\frac{\partial w_0(x,y)}{\partial x}-\Psi(z)\frac{\partial \psi(x,y)}{\partial x}$$
$$v(x,y,z)=\left(1+\frac{z}{R_y}\right)v_0(x,y)-z\frac{\partial w_0(x,y)}{\partial y}-\Psi(z)\frac{\partial \psi(x,y)}{\partial y} \quad (10)$$
$$w(x,y,z)=w_0(x,y)$$

In this theory, u, v, and w represent the displacements along the x, y, and z directions, respectively. ψ is the rotations. The specific form of the shape functions $\Psi(z)$ used is proposed as follows:

$$\Psi(z)=5h\tan^{-1}(z/h)-4z \quad (11)$$

Given the adjusted displacement field outlined in Eq. (10), the strains at any general point within the nanoshell's domain can be represented using the following formulation:

$$\begin{Bmatrix}\varepsilon_{xx}\\ \varepsilon_{yy}\\ \gamma_{xy}\\ \gamma_{yz}\\ \gamma_{xz}\end{Bmatrix}=\begin{bmatrix}u_{0,x}+w_0/R_x & -w_{0,xx} & \psi_{,xx} & 0 & 0\\ v_{0,y}+w_0/R_y & -w_{0,yy} & \psi_{,yy} & 0 & 0\\ v_{0,x}+u_{0,y} & -2w_{0,xy} & -2\psi_{,xy} & 0 & 0\\ 0 & 0 & 0 & \phi_{,y}-\psi_{,y} & 0\\ 0 & 0 & 0 & \phi_{,x}-\psi_{,x} & 0\end{bmatrix}\begin{Bmatrix}1\\ z\\ \Psi(z)\\ \Psi'(z)\\ \Psi''(z)\end{Bmatrix} \quad (12)$$

4. Nonlocal strain gradient elasticity theory

Incorporating the effects of strain gradient stress and nonlocal elastic stress, the constitutive equation for the nanoshell can be described as follows, according to Lim *et al*. (2015):

$$\sigma_{ij}=\sigma_{ij}^{(0)}-\frac{d\sigma_{ij}^{(1)}}{dx} \quad (13)$$

The stress $\sigma_{ij}^{(0)}$ and the higher-order stress $\sigma_{ij}^{(1)}$ are dependent on the strain ε_{kl} and the first-order strain gradient $\varepsilon_{kl,x}$ and they can be written as

The stress $\sigma_{ij}^{(0)}$ and the higher-order stress $\sigma_{ij}^{(1)}$ are influenced by the strain ε_{kl} and the first-order strain gradient $\varepsilon_{kl,x}$ and can be formulated as:

$$\sigma_{ij}^{(0)}=\int_0^L C_{ijkl}\alpha_0(x,x',e_0a)\varepsilon_{kl}(x')\mathrm{d}x'$$
$$\sigma_{ij}^{(1)}=l^2\int_0^L C_{ijkl}\alpha_1(x,x',e_1a)\varepsilon_{kl,x}(x')\mathrm{d}x' \quad (14)$$

The C_{ijkl} are the elastic constants, where l denotes the material length scale parameter that distinguishes the strain gradient stress field. The nonlocal parameters e_0a and e_1a define the nonlocal elastic stress field, with $\alpha\alpha_0(x,x',e_0a)$ and $\alpha_1(x,x',e_1a)$ representing the nonlocal kernel functions (Eringen 1984). The constitutive relation is expressed as:

$$[1-(e_1a)^2\nabla^2][1-(e_0a)^2\nabla^2]\sigma_{ij}$$
$$=C_{ijkl}[1-(e_1a)^2\nabla^2]\varepsilon_{kl}-C_{ijkl}l^2[1-(e_0a)^2\nabla^2]\nabla^2\varepsilon_{kl} \quad (15)$$

The nonlocal strain gradient constitutive relations given in Eq. (12) by assuming that $e=e_0=e_1$, can be presented as:

The nonlocal strain gradient constitutive relations, as provided in Eq. (12) with the assumption that $e=e_0=e_1$, can be expressed as:

$$[1-\mu\nabla^2]\sigma_{ij}=C_{ijkl}[1-\lambda\nabla^2]\varepsilon_{kl} \quad (16)$$

where $\mu=(ea)^2$ and $\lambda=l^2$.

The nonlocal strain gradient constitutive stress-strain relations are governed by (Daikh *et al*., 2024):

$$\begin{Bmatrix}\sigma_{xx}-\mu\nabla^2\sigma_{xx}\\ \sigma_{yy}-\mu\nabla^2\sigma_{yy}\\ \tau_{yz}-\mu\nabla^2\tau_{yz}\\ \tau_{xz}-\mu\nabla^2\tau_{xz}\\ \tau_{xy}-\mu\nabla^2\tau_{xy}\end{Bmatrix}=\begin{bmatrix}Q_{11} & Q_{12} & 0 & 0 & 0\\ Q_{12} & Q_{22} & 0 & 0 & 0\\ 0 & 0 & Q_{44} & 0 & 0\\ 0 & 0 & 0 & Q_{55} & 0\\ 0 & 0 & 0 & 0 & Q_{66}\end{bmatrix}\begin{Bmatrix}\varepsilon_{xx}-\lambda\nabla^2\varepsilon_{xx}\\ \varepsilon_{yy}-\lambda\nabla^2\varepsilon_{yy}\\ \gamma_{yz}-\lambda\nabla^2\gamma_{yz}\\ \gamma_{xz}-\lambda\nabla^2\gamma_{xz}\\ \gamma_{xy}-\lambda\nabla^2\gamma_{xy}\end{Bmatrix} \quad (17)$$

where

$$Q_{11}=Q_{22}=\frac{E(x,y,z)}{1-\upsilon^2}$$
$$Q_{12}=\upsilon Q_{11} \quad (18)$$
$$Q_{44}=Q_{55}=Q_{66}=\frac{E(x,y,z)}{2(1+\upsilon)}$$

$\mu=(ea)^2$, with ea representing the nonlocal effects, and $=l^2$, where l accounts for the strain gradient effects.

5. Equilibrium equations

The variational principle is employed to derive the equilibrium equations for GRNC shells, leading to the following formulation:

$$\int_V \sigma_{ij}\delta\varepsilon_{ij}\mathrm{d}V-\int_A q\delta w\mathrm{d}A-\int_A\left[N_{cr}\frac{\partial w_0}{\partial x}\frac{\partial\delta w_0}{\partial x}\right]\mathrm{d}A=0 \quad (19)$$

q represents the external transverse load. N_{cr} is the applied in-plane loads in the x-direction. The elastic foundation is described using two shear parameters that indicate the orthotropy directions, extending the Pasternak model (Kutlu and Omurtag 2012).

$$f_e=-G_\eta\left[\cos^2(\theta)\frac{\partial^2 w}{\partial x^2}+2cos(\theta)sin(\theta)\frac{\partial^2 \mathrm{w}}{\partial x\partial y}+\sin^2(\theta)\frac{\partial^2 \mathrm{w}}{\partial y^2}\right]$$
$$-G_\xi\left[\sin^2(\theta)\frac{\partial^2 \mathrm{w}}{\partial x^2}-2sin(\theta)cos(\theta)\frac{\partial^2 \mathrm{w}}{\partial x\partial y}+\cos^2(\theta)\frac{\partial^2 \mathrm{w}}{\partial y^2}\right] \quad (20)$$

G_η and G_ξ represent the shear foundation parameters in the η and ξ directions, respectively (see Fig. 3). Additionally, θ signifies the direction of orthotropy.

Based on the above equations, the equilibrium equations for the GRNC nanoshell, according to the proposed assumption, are derived as follows:

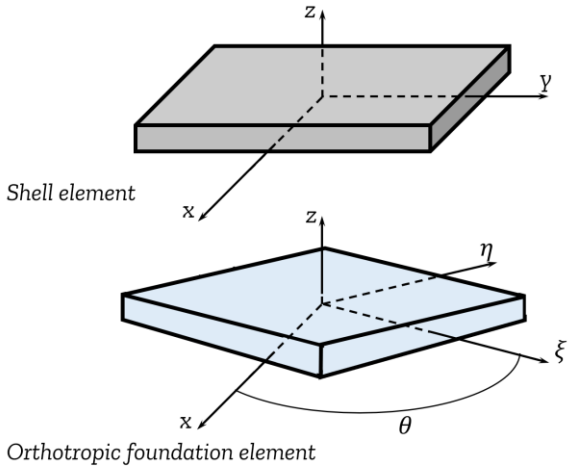

Fig. 3 Characterization of the orthotropic elastic foundation

account various boundary conditions. The Galerkin expressions for displacements can be stated as follows (Basha *et al*. 2022):

U_{mn}, V_{mn}, W_{mn} and Ψ_{mn} are arbitrary parameters, with m and n being mode numbers (both m=n=1). The functions $X_m(x)$ and $Y_n(y)$ that fulfill the simply supported and clamped boundary conditions are presented as follows:

$$\begin{aligned} u_0 &= \sum_{m=1}^{\infty}\sum_{n=1}^{\infty} U_{mn}.\frac{\partial X_m(x)}{\partial x}Y_n(y) \\ v_0 &= \sum_{m=1}^{\infty}\sum_{n=1}^{\infty} V_{mn}.X_m(x)\frac{\partial Y_n(y)}{\partial y} \\ \{w_0,\psi\} &= \sum_{m=1}^{\infty}\sum_{n=1}^{\infty}\{W_{mn},\Psi_{mn},\}X_m(x)Y_n(y) \end{aligned} \tag{27}$$

$$\begin{aligned}(1-\lambda\nabla^2)\Big[&A_{11}\frac{\partial^2 u_0}{\partial x^2}+A_{66}\frac{\partial^2 u_0}{\partial y^2}+(A_{12}+A_{66})\frac{\partial^2 v_0}{\partial x\partial y}+\left(\frac{A_{11}}{R_x}+\frac{A_{12}}{R_y}\right)\frac{\partial w_0}{\partial x}-B_{11}\frac{\partial^3 w_0}{\partial x^3}\\&-(B_{12}+2B_{66})\frac{\partial^3 w_0}{\partial x\partial y^2}-C_{11}\frac{\partial^3\psi}{\partial x^3}-(C_{12}+2C_{66})\frac{\partial^3\psi}{\partial x\partial y^2}\Big]=0\end{aligned} \tag{21}$$

$$\begin{aligned}(1-\lambda\nabla^2)\Big[&(A_{12}+A_{66})\frac{\partial^2 u_0}{\partial x\partial y}+A_{22}\frac{\partial^2 v_0}{\partial y^2}+A_{66}\frac{\partial^2 v_0}{\partial x^2}-(B_{12}+2B_{66})\frac{\partial^3 w_0}{\partial x^2\partial y}-B_{22}\frac{\partial^3 w_0}{\partial y^3}\\&+\left(\frac{A_{12}}{R_x}+\frac{A_{22}}{R_y}\right)\frac{\partial w_0}{\partial x}-(C_{12}+2C_{66})\frac{\partial^3\psi}{\partial x^2\partial y}-C_{22}\frac{\partial^3\psi}{\partial y^3}\Big]=0\end{aligned} \tag{22}$$

$$\begin{aligned}(1-\lambda\nabla^2)\Big[&B_{11}\frac{\partial^3 u_0}{\partial x^3}+(B_{12}+2B_{66})\frac{\partial^3 u_0}{\partial x\partial y^2}-\left(\frac{A_{11}}{R_x}+\frac{A_{12}}{R_y}\right)\frac{\partial u_0}{\partial x}+(B_{12}+2B_{66})\frac{\partial^3 v_0}{\partial x^2\partial y}+B_{22}\frac{\partial^3 v_0}{\partial y^3}\\&-\left(\frac{A_{12}}{R_x}+\frac{A_{22}}{R_y}\right)\frac{\partial v_0}{\partial y}+\left(\frac{2B_{11}}{R_x}+\frac{2B_{12}}{R_y}\right)\frac{\partial^2 w_0}{\partial x^2}-D_{11}\frac{\partial^4 w_0}{\partial x^4}-(2D_{12}+4D_{66})\frac{\partial^4 w_0}{\partial x^2\partial y^2}-D_{22}\frac{\partial^4 w_0}{\partial y^4}\\&+\left(\frac{2B_{12}}{R_x}+\frac{2B_{22}}{R_y}\right)\frac{\partial^2 w_0}{\partial y^2}-\left(\frac{A_{11}}{{R_x}^2}+2\frac{A_{12}}{R_xR_y}+\frac{A_{22}}{{R_y}^2}\right)w_0-E_{11}\frac{\partial^4\psi}{\partial x^4}-2(E_{12}+2E_{66})\frac{\partial^4\psi}{\partial x^2\partial y^2}\\&-E_{22}\frac{\partial^4\psi}{\partial y^4}+\left(\frac{C_{11}}{R_x}+\frac{C_{12}}{R_y}\right)\frac{\partial^2\psi}{\partial x^2}+\left(\frac{C_{12}}{R_x}+\frac{C_{22}}{R_y}\right)\frac{\partial^2\psi}{\partial y^2}\Big]+(1-\mu\nabla^2)\left[q-fe+\bar{N}^0_{xx}\frac{\partial^2 \mathrm{w}}{\partial x^2}+\bar{N}^0_{yy}\frac{\partial^2 w_0}{\partial y^2}\right]=0\end{aligned} \tag{23}$$

$$\begin{aligned}(1-\lambda\nabla^2)\Big[&C_{11}\frac{\partial^3 u}{\partial x^3}+(C_{12}+2C_{66})\frac{\partial^3 u}{\partial x\partial y^2}+(C_{12}+2C_{66})\frac{\partial^3 v}{\partial x^2\partial y}+C_{22}\frac{\partial^3 v}{\partial y^3}-E_{11}\frac{\partial^4 w_0}{\partial x^4}\\&-2(E_{12}+2E_{66})\frac{\partial^4 w_0}{\partial x^2\partial y^2}-E_{22}\frac{\partial^4 w_0}{\partial x^4}-F_{11}\frac{\partial^4\psi}{\partial x^4}-2(F_{12}+2F_{66})\frac{\partial^4\psi}{\partial x^2\partial y^2}\\&-F_{22}\frac{\partial^4\psi}{\partial y^4}+J_{44}\frac{\partial^2\psi}{\partial y^2}+J_{55}\frac{\partial^2\psi}{\partial x^2}+\left(\frac{C_{11}}{R_x}+\frac{C_{12}}{R_y}\right)\frac{\partial^2 w}{\partial x^2}+\left(\frac{C_{12}}{R_x}+\frac{C_{22}}{R_y}\right)\frac{\partial^2 w}{\partial y^2}\Big]=0\end{aligned} \tag{24}$$

The stiffness coefficients can be expressed as:

$$\begin{aligned}\{A_{ij},B_{ij},D_{ij},C_{ij},F_{ij},H_{ij}\}&=\int Q_{ij}\{1,z,z^2,f(z),zf(z),f(z)^2\}dxdydz\,,(i,j=1,2,6)\\ J_{ii}&=\int Q_{ii}\big(f'(z)\big)^2dxdydz,\quad(i=4,5)\end{aligned} \tag{25}$$

$$\{I_0,I_1,I_2,I_3,I_4,I_5\}=\rho(x,y,z)\left\{1,z,z^2,f(z),zf(z),\big(\Phi(z)\big)^2\right\}dxdydz \tag{26}$$

6. Analytical solution

Using the four-variable HSDT, an analytical solution is developed through the Galerkin approach, taking into

For SSSS shells: $X_m(x)=\sin(\alpha x)$ and $Y_n(y)=\sin(\beta y)$.

For CCCC shells: $X_m(x)=\sin^2(\alpha x)$ and $Y_n(y)=\sin^2(\beta y)$.

Table 1 Comparison of dimensionless critical buckling loads ($\times 10^{-2}$) for a GRNC plate subjected to uniaxial compressive in-plane loading (h=0.045m, a=10h, a_{GPL}=2.5μm, h_{GPL}=1.5nm, and w_{GPL}=1.5μm)

Pattern	g^*_{GPL}	SSSS				CCCC				CSCS		
		Gholami (2019)	Wu *et al*. (2018)	Thai *et al* (2020)	Present	Gholami (2019)	Wu *et al*. (2018)	Thai *et al* (2020)	Present	Gholami (2019)	Wu *et al*. (2018)	Present
UD-GRNC	0.1	0.0414	0.0413	0.0412	0.0413	0.0906	0.0899	0.0910	0.0927	0.0697	0.0692	0.0697
	0.3	0.0620	0.0619	0.0618	0.0620	0.1351	0.1346	0.1469	0.1259	0.1041	0.1037	0.0983
	0.5	0.0826	0.0825	0.0824	0.0827	0.1801	0.1794	0.1957	0.1586	0.1386	0.1382	0.1311
X-GRNC	0.1	0.0462	0.0460	0.0448	0.0450	0.0987	0.0984	0.1044	0.1083	0.0761	0.0760	0.0707
	0.3	0.0759	0.0758	0.0726	0.0728	0.1599	0.1597	0.1655	0.1722	0.1238	0.1235	0.1130
	0.5	0.1057	0.1055	0.1003	0.1004	0.2211	0.2207	0.2262	0.2353	0.1721	0.1709	0.1548
O-GRNC	0.1	0.0368	0.0366	0.0376	0.0376	0.0811	0.0809	0.0910	0.0927	0.0626	0.0622	0.0601
	0.3	0.0480	0.0478	0.0509	0.0504	0.1084	0.1072	0.1252	0.1259	0.0828	0.0823	0.0813
	0.5	0.0592	0.0588	0.0641	0.0632	0.1348	0.1331	0.1590	0.1586	0.1026	0.1021	0.1022
Pure epoxy	0	0.0311	0.0310	0.0309	0.0310	0.0680	0.0675	0.0735	0.0757	0.0523	0.0520	0.0492

For CSCS shells: $X_m(x) = \sin(\alpha x)[\cos(\alpha x) - 1]$ and $Y_n(y) = \sin(\beta y)[\cos(\beta y) - 1]$.

where $\lambda = m\pi/a,\ \mu = n\pi/b$.

By substituting Galerkin expressions represented in Eq. (27) into equilibrium Eqs. (21)-(24), one obtains

$$[K]_{5\times5}\begin{Bmatrix} U_{mn} \\ V_{mn} \\ W_{mn} \\ \Psi_{mn} \\ \Phi_{mn} \end{Bmatrix} = \begin{Bmatrix} 0 \\ 0 \\ q \\ 0 \\ 0 \end{Bmatrix} \tag{28}$$

K_{ij} elements of the mass matrix [K] are detailed in Appendix A.

The applied load follows a sinusoidal distribution and can be expressed as described by Thai *et al*. (2014):

$$\begin{aligned} q = &-q_0 \int_0^a \int_0^b \sin^2(\alpha x)\sin^2(\beta y)\,\mathrm{d}x\mathrm{d}y - \\ &\mu q_0 \left[\int_0^a \int_0^b \alpha^2 sin^2(\alpha x)\sin^2(\beta y)\,\mathrm{d}x\mathrm{d}y \right. \\ &\left. + \int_0^a \int_0^b \beta^2 \sin^2(\alpha x)\sin^2(\beta y)\,\mathrm{d}x\mathrm{d}y\right] \end{aligned} \tag{29}$$

where q_0 is the maximum load intensity.

7. Numerical results

The nanocomposite shell under consideration consists of an epoxy matrix with GPLs as reinforcement. The nanoshell is subjected to in-plane load in x-directions N_{cr} for buckling analysis, and a transverse sinusoidal load for bending analysis. The mechanical properties of the matrix and the GPL reinforcements are provided as follows:

Epoxy (matrix): $E_m = 3$ Gpa , $\nu_{\mathrm{m}} = 0.34$, $\rho_m = 1200\ \mathrm{kg/m^3}$.

GPLs (reinforcement): $E_{\mathrm{GPL}} = 1010$ Gpa , $\nu_{\mathrm{GPL}} = 0.186$, $\rho_{\mathrm{GPL}} = 1060\ \mathrm{kg/m^3}$.

The composite nanoshell is composed of GPLs with a length $aa_{\mathrm{GPL}} = 2.5$ μm, a thickness $\mathrm{h_{GPL}} = 1.5$ nm, and a width $\mathrm{h_{GPL}} = 1.5$ nm. The normalized critical buckling load $\bar{N}$ and displacement $\bar{w}$ are assessed using the following expressions:

$$\bar{N} = 10^2 \frac{N_{cr}(1-\nu_m)}{E_m h} \tag{30}$$

$$\bar{w} = \frac{10h}{a^2 q_0} w\left(\frac{a}{2}, \frac{b}{2}, z\right) \tag{31}$$

To confirm the accuracy of the proposed model, the current results are compared with those from Wu *et al*. (2018), Gholami and Ansari (2019), and Thai *et al*. (2020) as shown in Table 2, demonstrating that the proposed solutions align well with these previous findings for functionally graded graphene reinforced composite square plates with specific dimensions and boundary conditions. The comparison indicates that the proposed solutions align well with the results from other studies.

7.1 Impact of material properties

Tables 2 and 3 and Fig. 4 present the effects of material properties - represented by the weight fraction "g^*_{GPL}," reinforcement patterns of GPLs, and the inhomogeneity parameter "N" - on the static response of doubly curved GNRC shells. The findings reveal that shell stiffness improves with an increase in weight fraction, a rise in the inhomogeneity parameter for FG-A CNRC shells, and a decrease in the inhomogeneity parameter for FG-B CNRC shells. Consequently, this leads to a reduction in dimensionless central deflection and an increase in dimensionless critical buckling load.

7.2 Impact of geometric parameters

Tables 4 and 5, along with Fig. 5, illustrate the impact of shell geometry on the dimensionless central deflection and critical buckling load of simply supported GRNC shells with various GPL reinforcement patterns. The results

Table 2 Effect of weight fraction g^*_{GPL} and shell radius on the dimensionless central deflection of simply supported square GRNC shells for various GPLs reinforcement patterns (a=b=10h)

Pattern	N	R	g^*_{GPL}					
			0	0,2	0,4	0,6	0,8	1
UD		5	8.6253	5.1792	3.7011	2.8796	2.3567	1.9947
		10	9.3512	5.6152	4.0128	3.1222	2.5553	2.1627
		20	9.5521	5.7359	4.0990	3.1893	2.6102	2.2093
		50	9.6100	5.7707	4.1239	3.2086	2.6261	2.2227
		10	9.6183	5.7757	4.1274	3.2114	2.6283	2.2246
FG-A	1	5	8.6253	6.5126	5.2579	4.4136	3.8045	3.3439
		10	9.3512	7.2172	5.9099	5.0100	4.3501	3.8447
		20	9.5521	7.4178	6.0990	5.1852	4.5119	3.9943
		50	9.6100	7.4760	6.1541	5.2365	4.5594	4.0383
		10	9.6183	7.4844	6.1620	5.2439	4.5662	4.0447
	2	5	8.6253	5.4780	4.0142	3.1682	2.6169	2.2292
		10	9.3512	5.9681	4.3834	3.4642	2.8640	2.4413
		20	9.5521	6.1047	4.4866	3.5471	2.9332	2.5007
		50	9.6100	6.1440	4.5164	3.5710	2.9532	2.5179
		10	9.6183	6.1497	4.5207	3.5744	2.9561	2.5204
	3	5	8.6253	5.3086	3.8348	3.0019	2.4665	2.0934
		10	9.3512	5.7676	4.1704	3.2665	2.6849	2.2793
		20	9.5521	5.8950	4.2637	3.3400	2.7456	2.3310
		50	9.6100	5.9317	4.2906	3.3612	2.7631	2.3459
		10	9.6183	5.9370	4.2945	3.3643	2.7656	2.3481
FG-B	1	5	8.6253	4.3631	2.9404	2.2231	1.7892	1.4980
		10	9.3512	4.6684	3.1338	2.3649	1.9014	1.5909
		20	9.5521	4.7515	3.1861	2.4032	1.9317	1.6159
		50	9.6100	4.7754	3.2011	2.4142	1.9403	1.6231
		10	9.6183	4.7788	3.2033	2.4158	1.9416	1.6241
	2	5	8.6253	4.9122	3.4347	2.6409	2.1454	1.8066
		10	9.3512	5.3027	3.7015	2.8435	2.3087	1.9434
		20	9.5521	5.4102	3.7748	2.8990	2.3535	1.9809
		50	9.6100	5.4411	3.7958	2.9150	2.3663	1.9917
		10	9.6183	5.4456	3.7988	2.9173	2.3682	1.9932
	3	5	8.6253	5.0565	3.5773	2.7681	2.2576	1.9064
		10	9.3512	5.4713	3.8676	2.9914	2.4392	2.0593
		20	9.5521	5.5858	3.9477	3.0530	2.4892	2.1014
		50	9.6100	5.6187	3.9707	3.0707	2.5036	2.1136
		10	9.6183	5.6235	3.9741	3.0733	2.5057	2.1153

Table 3 Effect of shell radius and g^*_{GPL} weight fraction on the dimensionless critical buckling load of simply supported square GRNC shells for various GPLs reinforcement patterns

Pattern	N	R	g^*_{GPL}					
			0	0,2	0,4	0,6	0,8	1
UD		5	3.4630	5.7672	8.0704	10.3727	12.6741	14.9746
		10	3.1942	5.3194	7.4436	9.5670	11.6894	13.8109
		20	3.1270	5.2074	7.2869	9.3655	11.4432	13.5200
		50	3.1082	5.1761	7.2431	9.3091	11.3743	13.4386
		10	3.1055	5.1716	7.2368	9.3011	11.3645	13.4269

Table 3 Continued

		5	3.4630	4.5864	5.6809	6.7677	7.8511	8.9326
		10	3.1942	4.1387	5.0542	5.9619	6.8664	7.7689
	1	20	3.1270	4.0267	4.8975	5.7605	6.6202	7.4780
		50	3.1082	3.9954	4.8536	5.7041	6.5513	7.3965
		10	3.1055	3.9909	4.8473	5.6960	6.5414	7.3849
		5	3.4630	5.4526	7.4409	9.4280	11.4140	13.3989
		10	3.1942	5.0049	6.8142	8.6223	10.4293	12.2352
FG-A	2	20	3.1270	4.8929	6.6575	8.4209	10.1831	11.9443
		50	3.1082	4.8616	6.6136	8.3645	10.1142	11.8628
		10	3.1055	4.8571	6.6073	8.3564	10.1044	11.8512
		5	3.4630	5.6266	7.7890	9.9500	12.1099	14.2685
		10	3.1942	5.1788	7.1622	9.1443	11.1252	13.1048
	3	20	3.1270	5.0669	7.0055	8.9429	10.8790	12.8139
		50	3.1082	5.0356	6.9616	8.8865	10.8100	12.7324
		10	3.1055	5.0311	6.9554	8.8784	10.8002	12.7208
		5	3.4630	6.8460	10.1583	13.4361	16.6940	19.9390
		10	3.1942	6.3982	9.5315	12.6304	15.7093	18.7753
	1	20	3.1270	6.2863	9.3749	12.4289	15.4631	18.4844
		50	3.1082	6.2549	9.3310	12.3725	15.3942	18.4029
		10	3.1055	6.2505	9.3247	12.3645	15.3843	18.3913
		5	3.4630	6.0807	8.6964	11.3104	13.9227	16.5333
		10	3.1942	5.6329	8.0696	10.5047	12.9380	15.3696
FG-B	2	20	3.1270	5.5209	7.9130	10.3032	12.6918	15.0787
		50	3.1082	5.4896	7.8691	10.2468	12.6229	14.9972
		10	3.1055	5.4851	7.8628	10.2388	12.6130	14.9856
		5	3.4630	5.9071	8.3497	10.7908	13.2303	15.6684
		10	3.1942	5.4594	7.7230	9.9850	12.2456	14.5047
	3	20	3.1270	5.3474	7.5663	9.7836	11.9994	14.2138
		50	3.1082	5.3161	7.5224	9.7272	11.9305	14.1323
		10	3.1055	5.3116	7.5161	9.7191	11.9207	14.1207

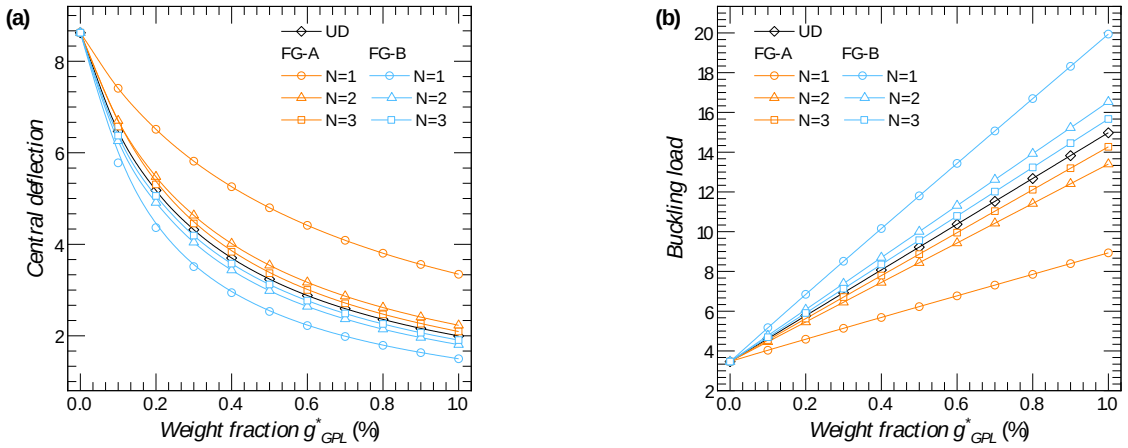

Fig. 4 Effect of weight fraction on the mechanical response of simply supported square doubly-curved GRNC shells (a/h=10, R=5)

indicate that increases in both the aspect ratio b/a and the thickness ratio a/h lead to higher dimensionless central deflection and lower dimensionless critical buckling loads. Additionally, the FG-B CNRC shell exhibits greater rigidity

Table 4 Effect of shell geometry on the dimensionless central deflection of simply supported GRNC shells for various GPLs reinforcement patterns (g^*_{GPL}=1%)

a/*h*	*b*/*a*	UD	FG-A			FG-A		
			N=1	*N*=2	*N*=3	*N*=1	*N*=2	*N*=3
5	0.5	0.1323	0.1964	0.1500	0.1400	0.1317	0.1188	0.1255
	1	0.6285	1.0315	0.7096	0.6628	0.5340	0.5652	0.5981
	2	1.5006	2.5612	1.6944	1.5821	1.1959	1.3485	1.4282
	5	2.1689	3.8052	2.4560	2.2893	1.6851	1.9446	2.0622
10	0,5	0.3751	0.6403	0.4236	0.3955	0.2990	0.3371	0.3570
	1	1.9947	3.3439	2.2292	2.0934	1.4980	1.8066	1.9064
	2	5.0500	8.6080	5.6502	5.3021	3.6995	4.5694	4.8247
	5	7.8341	14.2000	8.8495	8.2581	5.5796	7.0347	7.4581
20	0.5	1.2625	2.1520	1.4126	1.3255	0.9249	1.1424	1.2062
	1	5.9090	8.7000	6.4315	6.1317	4.5289	5.4687	5.7055
	2	15.4394	23.0577	16.8435	16.0368	11.6994	14.2609	14.8945
	5	28.8135	50.3663	32.2970	30.2727	20.3465	26.0304	27.5117
30	0.5	2.4996	4.0054	2.7629	2.6108	1.8444	2.2838	2.3992
	1	9.5693	12.4926	10.1685	9.8280	7.7898	9.0409	9.3279
	2	25.4578	33.6816	27.1227	26.1755	20.5253	23.9967	24.7899
	5	58.7456	96.3797	65.1382	61.4394	42.4107	53.5362	56.3213

Table 5 Effect of shell geometry on the dimensionless critical buckling load of simply supported GRNC shells for various GPLs reinforcement patterns (g^*_{GPL}=1%)

a/*h*	*b*/*a*	UD	FG-A			FG-A		
			N=1	*N*=2	*N*=3	*N*=1	*N*=2	*N*=3
5	0.5	225.7679	52.0882	199.0821	213.4104	226.8241	251.5221	237.9281
	1	47.5229	28.9575	42.0964	45.0656	55.9407	52.8495	49.9412
	2	19.9053	11.6621	17.6279	18.8795	24.9773	22.1496	20.9142
	5	13.7719	7.8497	12.1618	13.0477	17.7260	15.3604	14.4840
10	0,5	79.6212	46.6484	70.5118	75.5180	99.9093	88.5984	83.6568
	1	14.9746	8.9326	13.3989	14.2685	19.9390	16.5333	15.6684
	2	5.9147	3.4700	5.2864	5.6335	8.0739	6.5368	6.1909
	5	3.8128	2.1035	3.3753	3.6170	5.3534	4.2460	4.0050
20	0.5	23.6589	13.8798	21.1456	22.5340	32.2957	26.1473	24.7638
	1	5.0549	3.4333	4.6443	4.8713	6.5954	5.4619	5.2352
	2	1.9346	1.2954	1.7734	1.8626	2.5531	2.0945	2.0054
	5	1.0366	0.5930	0.9248	0.9867	1.4680	1.1475	1.0857
30	0.5	11.9499	7.4574	10.8110	11.4407	16.1945	13.0786	12.4500
	1	3.1214	2.3910	2.9375	3.0392	3.8344	3.3038	3.2022
	2	1.1733	0.8868	1.1013	1.1411	1.4553	1.2447	1.2049
	5	0.5085	0.3099	0.4586	0.4862	0.7043	0.5579	0.5303

compared to the UD and FG-A CNRC shells.

For a more detailed analysis, Fig. 6 illustrates the impact of the shell radius ratio *R* and the aspect ratio *b*/*a* on the mechanical response of doubly-curved FG-A GRNC shells. The results demonstrate that increasing the radius ratio *R* ($R=R_x/a= R_y/b$) leads to a decrease in shell stiffness. When *R* exceeds 20, the results stabilize and show minimal variation.

7.3 Impact of small-scale:

To examine the influence of size-dependence, represented by the nonlocal parameter and the length scale parameter, on the response of GRNC shells, refer to Tables 6 and 7 and

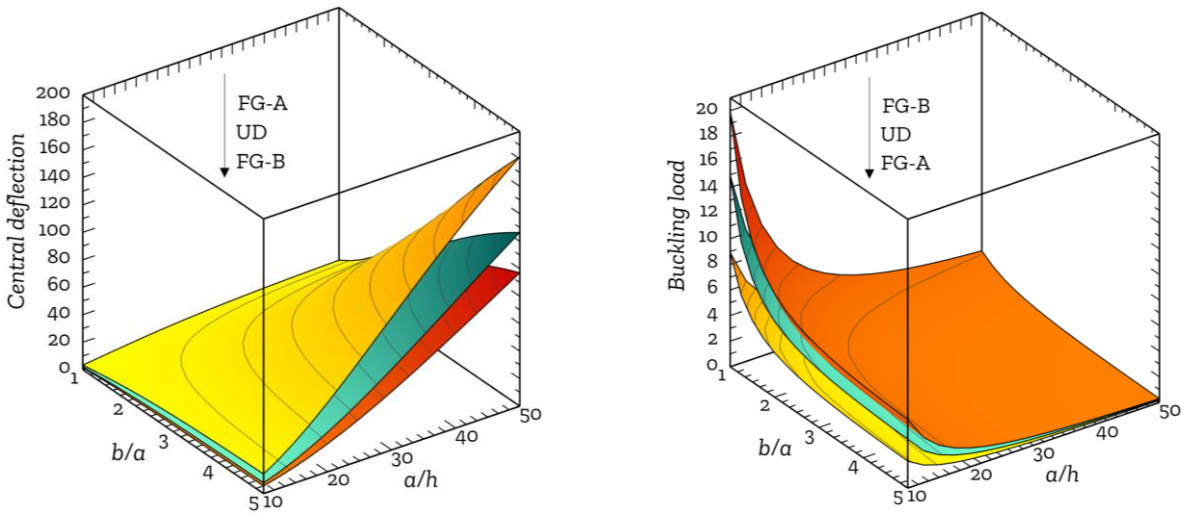

Fig. 5 Effect of geometrical parameters a/h and b/a on the mechanical response of simply supported doubly-curved GRNC shells (g^*_{GPL}=1%, *R*=5)

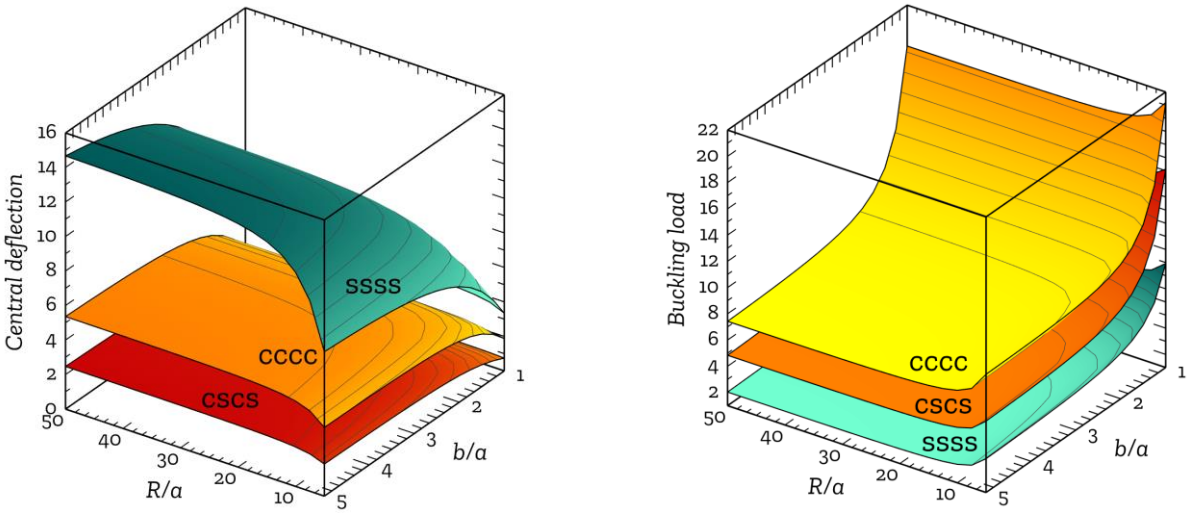

Fig. 6 Effect of geometrical parameters *R* and *b*/*a* on the mechanical response of doubly-curved FG-A GRNC shells (g^*_{GPL}=1%, *a*/*h*=10)

Table 6 Effect of nonlocal parameter and length scale parameter on the dimensionless central deflection of simply supported GRNC shells for various GPLs reinforcement patterns (g^*_{GPL}=1%, *a*=*b*=10*h*)

Pattern	λ	*μ*					
		0	0,2	0,4	0,6	0,8	1
UD	0.0	1.9947	2.0734	2.1522	2.2309	2.3097	2.3884
	0.2	1.9118	1.9873	2.0628	2.1382	2.2137	2.2892
	0.4	1.8365	1.9090	1.9815	2.0540	2.1265	2.1991
	0.6	1.7678	1.8376	1.9074	1.9771	2.0469	2.1167
	0.8	1.7047	1.7720	1.8393	1.9066	1.9739	2.0412
	1.0	1.6465	1.7115	1.7765	1.8415	1.9065	1.9715
FG-A	0.0	3.3439	3.4759	3.6079	3.7399	3.8719	4.0039
	0.2	3.1970	3.3232	3.4494	3.5756	3.7018	3.8280
	0.4	3.0652	3.1862	3.3072	3.4282	3.5492	3.6702
	0.6	2.9461	3.0624	3.1787	3.2950	3.4114	3.5277
	0.8	2.8378	2.9499	3.0619	3.1739	3.2860	3.3980
	1.0	2.7388	2.8469	2.9550	3.0631	3.1713	3.2794

Table 6 Continued

Pattern	λ	μ					
		0	0,2	0,4	0,6	0,8	1
FG-B	0.0	1.4980	1.5572	1.6163	1.6755	1.7346	1.7937
	0.2	1.4371	1.4939	1.5506	1.6074	1.6641	1.7208
	0.4	1.3816	1.4361	1.4906	1.5452	1.5997	1.6543
	0.6	1.3306	1.3831	1.4356	1.4882	1.5407	1.5932
	0.8	1.2836	1.3343	1.3850	1.4356	1.4863	1.5370
	1.0	1.2402	1.2891	1.3381	1.3870	1.4360	1.4850

Table 7 Effect of nonlocal parameter and length scale parameter on the dimensionless critical buckling load of simply supported GRNC shells for various GPLs reinforcement patterns (g^*_{GPL}=1%, a=b=10h)

Pattern	λ	μ					
		0	0,2	0,4	0,6	0,8	1
UD	0.0	14.9746	14.4059	13.8788	13.3889	12.9324	12.5060
	0.2	15.6237	15.0303	14.4804	13.9692	13.4930	13.0481
	0.4	16.2641	15.6464	15.0739	14.5418	14.0460	13.5829
	0.6	16.8966	16.2549	15.6602	15.1074	14.5923	14.1112
	0.8	17.5222	16.8567	16.2400	15.6667	15.1326	14.6336
	1.0	18.1415	17.4525	16.8139	16.2204	15.6674	15.1508
FG-A	0.0	8.9326	8.5934	8.2790	7.9867	7.7144	7.4601
	0.2	9.3430	8.9882	8.6593	8.3537	8.0689	7.8028
	0.4	9.7447	9.3746	9.0316	8.7128	8.4158	8.1383
	0.6	10.1386	9.7536	9.3967	9.0650	8.7559	8.4672
	0.8	10.5255	10.1258	9.7553	9.4109	9.0901	8.7904
	1.0	10.9061	10.4919	10.1080	9.7512	9.4188	9.1082
FG-B	0.0	19.9390	19.1818	18.4799	17.8276	17.2198	16.6521
	0.2	20.7839	19.9946	19.2630	18.5831	17.9495	17.3577
	0.4	21.6201	20.7990	20.0380	19.3307	18.6716	18.0560
	0.6	22.4485	21.5960	20.8058	20.0714	19.3871	18.7479
	0.8	23.2700	22.3862	21.5671	20.8058	20.0965	19.4339
	1.0	24.0851	23.1704	22.3226	21.5346	20.8004	20.1146

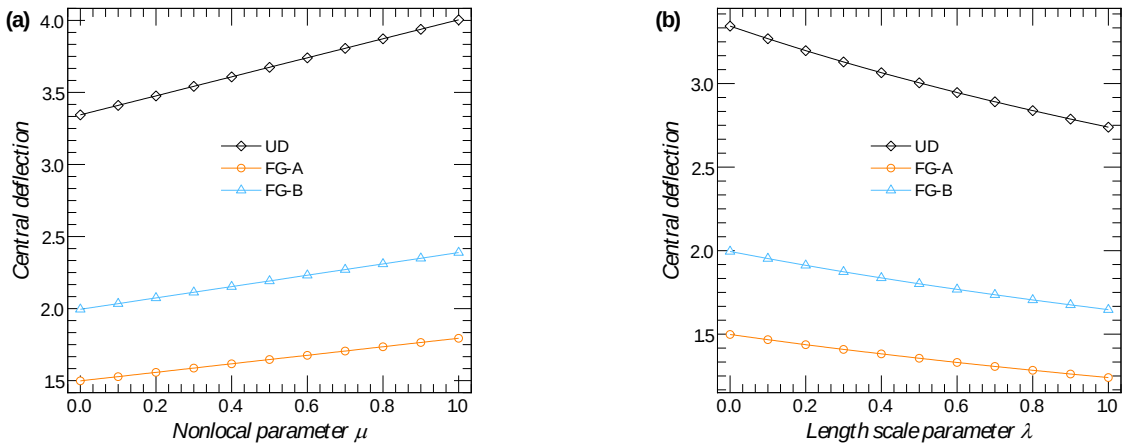

Fig. 7 Effect of nonlocal parameter and length scale parameter on the central deflection of simply supported square doubly-curved GRNC nanoshells (g^*_{GPL}=1%, a=b=10h, R=5)

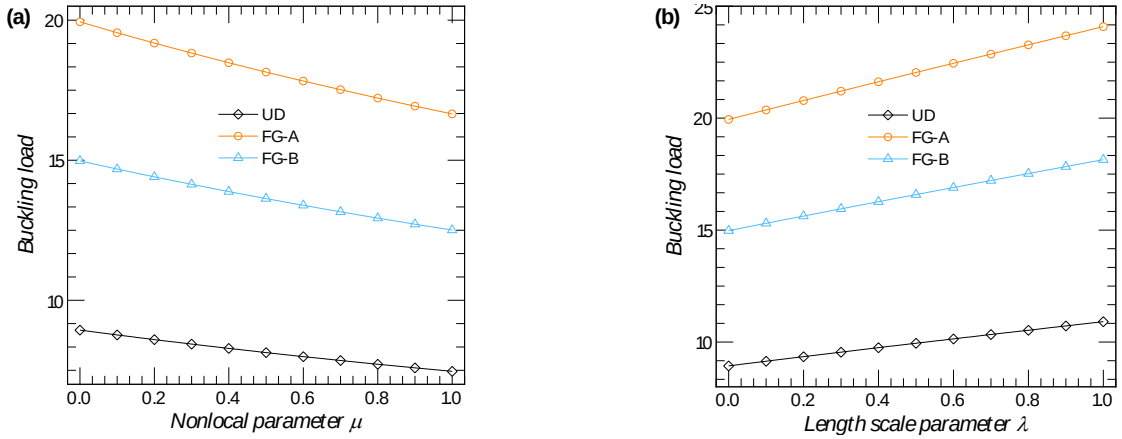

Fig. 8 Effect of nonlocal parameter and length scale parameter on the critical buckling load of simply supported square doubly-curved GRNC nanoshells (g^*_{GPL}=1%, a=b=10h, R=5)

Table 8 Effect of the orthotropic foundation parameters on the dimensionless central deflection of simply supported GRNC shells for various GPLs reinforcement patterns (g^*_{GPL}=1%, a=10h, b=3a)

Pattern	θ	G_ζ=5			G_ζ=5			G_ζ=5		
		G_η=5	G_η=10	G_η=10	G_η=5	G_η=10	G_η=10	G_η=5	G_η=10	G_η=10
UD	0°	6.0219	5.9662	5.8579	5.5552	5.5078	5.4153	4.8098	4.7742	4.7046
	30°	6.0219	5.8579	5.5552	5.6526	5.5078	5.2394	5.0350	4.9198	4.7046
	45°	6.0219	5.7534	5.2823	5.7534	5.5078	5.0746	5.2823	5.0746	4.7046
	60°	6.0219	5.6526	5.0350	5.8579	5.5078	4.9198	5.5552	5.2394	4.7046
	90°	6.0219	5.5552	4.8098	5.9662	5.5078	4.7742	5.8579	5.4153	4.7046
FG-A	0°	9.9045	9.7548	9.4685	8.7022	8.5864	8.3638	7.0022	6.9270	6.7814
	30°	9.9045	9.4685	8.7022	8.9435	8.5864	7.9515	7.4899	7.2378	6.7814
	45°	9.9045	9.1985	8.0507	9.1985	8.5864	7.5779	8.0507	7.5779	6.7814
	60°	9.9045	8.9435	7.4899	9.4685	8.5864	7.2378	8.7022	7.9515	6.7814
	90°	9.9045	8.7022	7.0022	9.7548	8.5864	6.9270	9.4685	8.3638	6.7814
FG-B	0°	4.4577	4.4271	4.3672	4.1967	4.1696	4.1164	3.7569	3.7351	3.6923
	30°	4.4577	4.3672	4.1967	4.2520	4.1696	4.0140	3.8929	3.8236	3.6923
	45°	4.4577	4.3088	4.0391	4.3088	4.1696	3.9165	4.0391	3.9165	3.6923
	60°	4.4577	4.2520	3.8929	4.3672	4.1696	3.8236	4.1967	4.0140	3.6923
	90°	4.4577	4.1967	3.7569	4.4271	4.1696	3.7351	4.3672	4.1164	3.6923

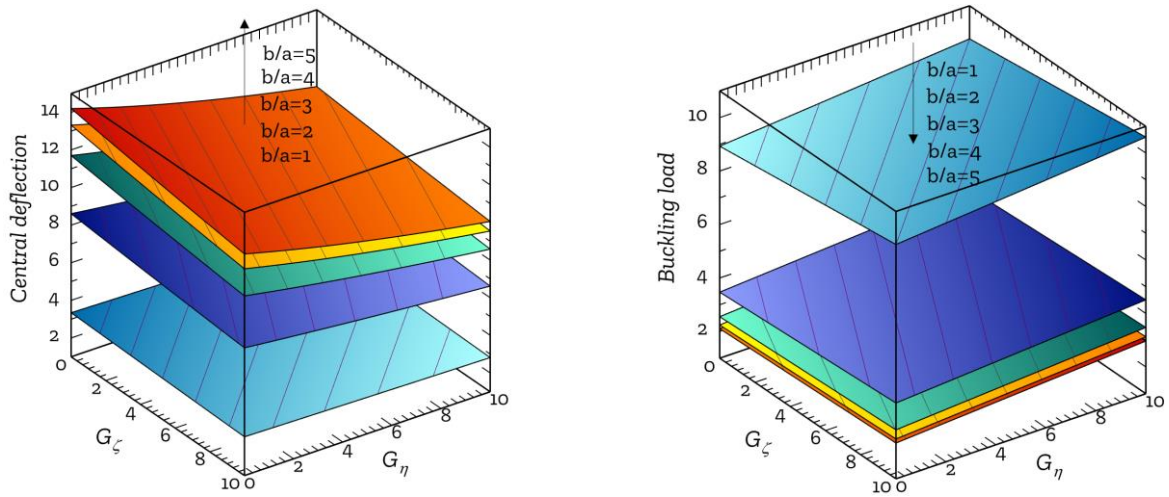

Fig. 9 Effect of the orthotropic elastic foundation parameters on the mechanical response of simply supported square doubly-curved FG-A GRNC shells (g^*_{GPL}=1%, θ=30°, R=5)

Table 9 Effect of the orthotropic foundation parameters on the dimensionless vritical buckling load of simply supported GRNC shells for various GPLs reinforcement patterns (g^*_{GPL}=1%, a=10h, b=3a)

Pattern	θ	G_ζ=5			G_ζ=5			G_ζ=5		
		G_η=5	G_η=10	G_η=10	G_η=5	G_η=10	G_η=10	G_η=5	G_η=10	G_η=10
UD	0°	4.9602	5.0065	5.0991	5.3768	5.4231	5.5157	6.2102	6.2565	6.3491
	30°	4.9602	5.0991	5.3768	5.2842	5.4231	5.7009	5.9324	6.0713	6.3491
	45°	4.9602	5.1916	5.6546	5.1916	5.4231	5.8861	5.6546	5.8861	6.3491
	60°	4.9602	5.2842	5.9324	5.0991	5.4231	6.0713	5.3768	5.7009	6.3491
	90°	4.9602	5.3768	6.2102	5.0065	5.4231	6.2565	5.0991	5.5157	6.3491
FG-A	0°	3.0157	3.0620	3.1546	3.4324	3.4787	3.5713	4.2657	4.3120	4.4046
	30°	3.0157	3.1546	3.4324	3.3398	3.4787	3.7565	3.9880	4.1269	4.4046
	45°	3.0157	3.2472	3.7102	3.2472	3.4787	3.9417	3.7102	3.9417	4.4046
	60°	3.0157	3.3398	3.9880	3.1546	3.4787	4.1269	3.4324	3.7565	4.4046
	90°	3.0157	3.4324	4.2657	3.0620	3.4787	4.3120	3.1546	3.5713	4.4046
FG-B	0°	6.7007	6.7470	6.8396	7.1174	7.1637	7.2562	7.9507	7.9970	8.0896
	30°	6.7007	6.8396	7.1174	7.0248	7.1637	7.4414	7.6729	7.8118	8.0896
	45°	6.7007	6.9322	7.3951	6.9322	7.1637	7.6266	7.3951	7.6266	8.0896
	60°	6.7007	7.0248	7.6729	6.8396	7.1637	7.8118	7.1174	7.4414	8.0896
	90°	6.7007	7.1174	7.9507	6.7470	7.1637	7.9970	6.8396	7.2562	8.0896

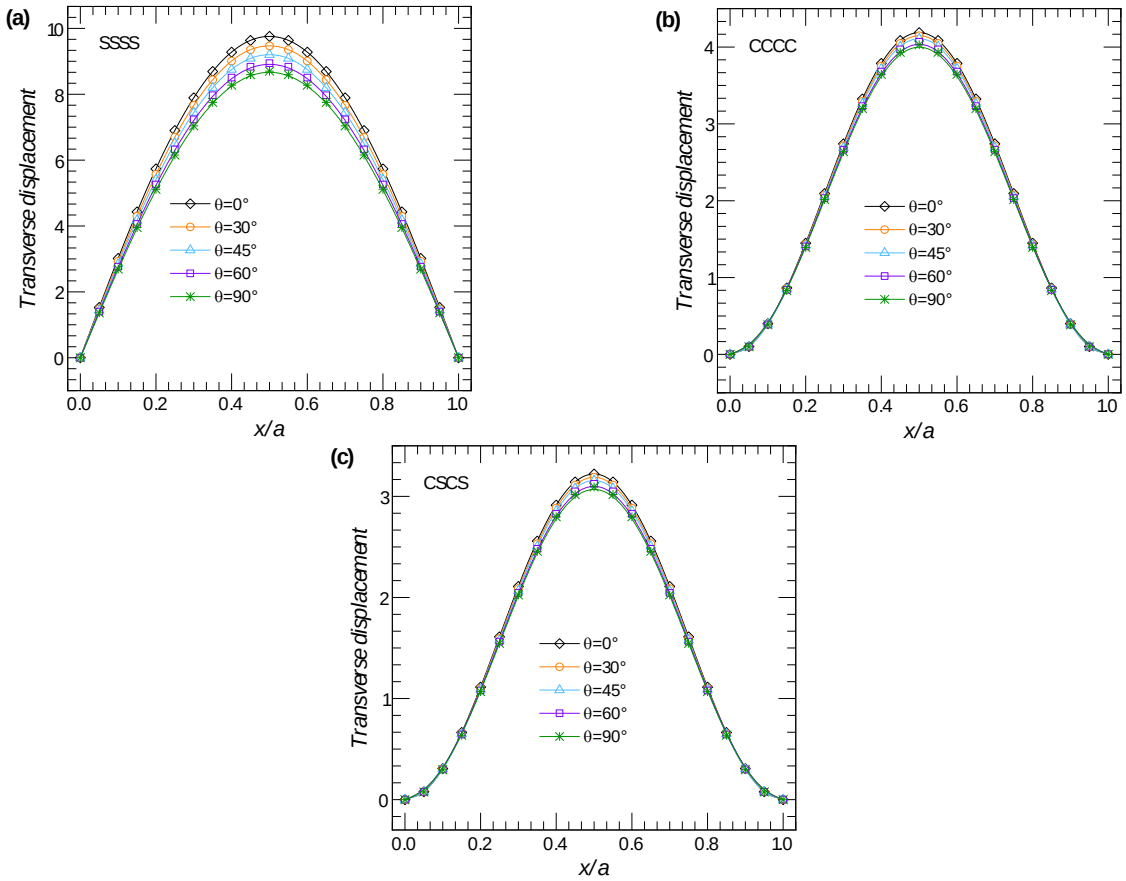

Fig. 9 Effect of the orientation angle on the transverse displacement of square doubly-curved FG-A GRNC shells (g^*_{GPL}=1%, a=10h, b=3a, R=5, G_ζ=5, G_η=10)

Figs. 7 and 8. The results indicate that, regardless of the GPLs reinforcement pattern, an increase in the nonlocal parameter results in reduced shell stiffness. This change leads to an increase in dimensionless central deflection and a decrease in dimensionless critical buckling load, in contrast to the effects of the length scale parameter.

7.4 Impact of elastic foundation:

In this subsection, we examine the mechanical response of simply supported GRNC shells with various GPL reinforcement patterns subjected to an orthotropic elastic foundation characterized by parameters G_ζ and G_η. The results are presented in Tables 8 and 9, and Figs. 9 and 10. Fig. 8 demonstrates that the inclusion of an elastic foundation enhances the stiffness of the shell, which leads to reduced deflections and a decrease in the critical buckling loads. Additionally, Fig. 9 illustrates how varying the foundation's orientation angle affects the transverse displacement of FG-A GRNC shells under different boundary conditions. An increase in the orientation angle improves the shell's stiffness, resulting in a reduction in the maximum point of displacement.

8. Conclusions

This paper explores the mechanical characteristics of cosine FG-GRNC laminated shells by utilizing an advanced higher-order shear deformation shell theory alongside a modified continuum nonlocal strain gradient approach. The investigation incorporates two graphene-reinforced distribution patterns; FG-A CNRCs and FG-B CNRCs, along with UD CNRCs. A thorough parametric study is conducted to analyze the impact of various factors, including the length scale parameter, material scale parameter, reinforcement distribution, GPL weight fraction, shell thickness, and geometry, on deflections and critical buckling loads. The credibility of the proposed solutions is established through comparisons with established results. Numerical findings reveal that:

• Shell stiffness increases with a higher weight fraction and a rise in the inhomogeneity parameter for FG-A CNRC shells, while it decreases with a lower inhomogeneity parameter for FG-B CNRC shells.

• An increase in both the aspect ratio (b/a) and the thickness ratio (a/h) results in greater dimensionless central deflection and lower dimensionless critical buckling loads.

• Increasing the radius (R) leads to a decrease in shell stiffness.

• For all GPL reinforcement patterns, an increase in the nonlocal parameter or a decrease in length scale parameters results in reduced shell stiffness.

• The inclusion of an elastic foundation enhances the shell's stiffness, leading to reduced deflections and decreased critical buckling loads.

Increasing the orientation angle of the reinforcement improves shell stiffness, resulting in reduced displacements.

Acknowledgment

This project was funded by the Deanship of Scientific Research (DSR) at King Abdulaziz University, Jeddah, under grand no. (GPIP: 78-135-2024). The Authors, therefore, acknowledge with thanks DSR for technical and financial support.

References

Affdl, J.H. and Kardos, J.L. (1976), "The Halpin–Tsai equations: A review", *Polym. Eng. Sci.*, **16**(5), 344-352. https://doi.org/10.1002/pen.760160512

Akbaş, Ş.D., Ersoy, H., Akgöz, B. and Civalek, Ö. (2021), "Dynamic analysis of a fiber-reinforced composite beam under a moving load by the Ritz method", *Mathematics*, **9**(9), 1048. https://doi.org/10.3390/math9091048

Alazwari, M.A., Daikh, A.A., Houari, M.S.A., Tounsi, A. and Eltaher, M.A. (2021), "On static buckling of multilayered carbon nanotube-reinforced composite nanobeams supported on nonlinear elastic foundations", *Steel Compos. Struct.*, **40**(3), 389-404. https://doi.org/10.12989/scs.2021.40.3.389

Alazwari, M.A., Esen, I., Abdelrahman, A.A., Abdraboh, A.M. and Eltaher, M.A. (2022), "Dynamic analysis of functionally graded (FG) nonlocal strain gradient nanobeams under thermo-magnetic fields and moving load", *Adv. Nano Res.*, **12**(3), 231-251. https://doi.org/10.12989/anr.2022.12.3.231

Basha, M., Daikh, A.A., Melaibari, A., Wagih, A., Othman, R., Almitani, K.H., Hamed, M.A., Abdelrahman, A. and Eltaher, M.A. (2022), "Nonlocal strain gradient theory for buckling and bending of FG-GRNC laminated sandwich plates", *Steel Compos. Struct.*, **43**(5), 639-660. https://doi.org/10.12989/scs.2022.43.5.639

Belarbi, M.O., Daikh, A.A., Garg, A., Hirane, H., Houari, M.S.A., Civalek, Ö. and Chalak, H.D. (2023), "Bending and free vibration analysis of porous functionally graded sandwich plates with various porosity distributions using an extended layerwise theory", *Arch. Civil Mech. Eng.*, **23**(1), 15. https://doi.org/10.1007/s43452-022-00551-0

Bouadi, A., Bousahla, A.A., Houari, M.S.A., Heireche, H. and Tounsi, A. (2018), "A new nonlocal HSDT for analysis of stability of single layer graphene sheet", *Adv. Nano Res.*, **6**(2), 147-162. http://dx.doi.org/10.12989/anr.2018.6.2.147

Civalek, Ö. and Avcar, M. (2022), "Free vibration and buckling analyses of CNT reinforced laminated non-rectangular plates by discrete singular convolution method", *Eng. Comput.*, **38**, 489-521. https://doi.org/10.1007/s00366-020-01168-8

Daikh, A.A., Belarbi, M.O., Khechai, A., Li, L., Ahmed, H.M. and Eltaher, M.A. (2023), "Buckling of bi-coated functionally graded porous nanoplates via a nonlocal strain gradient quasi-3D theory", *Acta Mechanica*, **234**, 3397-3420. https://doi.org/10.1007/s00707-023-03548-9

Daikh, A.A., Belarbi, M.O., Khechai, A., Li, L., Ahmed, H.M. and Eltaher, M.A. (2023), "Buckling of bi-coated functionally graded porous nanoplates via a nonlocal strain gradient quasi-3D theory", *Acta Mechanica*, **234**(8), 3397-3420. https://doi.org/10.1007/s00707-023-03548-9

Daikh, A.A., Belarbi, M.O., Vinh, P.V., Li, L., Houari, M.S.A. and Eltaher, M.A. (2024), "Vibration analysis of tri-directionally coated plates via thickness-stretching and micro-structure-dependent modeling", *Mech. Res. Commun.*, **135**, 104221. https://doi.org/10.1016/j.mechrescom.2023.104221

Daikh, A.A., Guerroudj, M., El Adjrami, M. and Megueni, A. (2019), "Thermal buckling of functionally graded sandwich beams", *Adv. Mater. Res.*, **1156**, 43-59. https://doi.org/10.4028/www.scientific.net/AMR.1156.43

Daikh, A.A., Houari, M.S.A., Belarbi, M.O., Mohamed, S.A. and Eltaher, M.A. (2022), "Static and dynamic stability responses of multilayer functionally graded carbon nanotubes reinforced composite nanoplates via quasi 3D nonlocal strain gradient theory", *Defence Technol.*, **18**(10), 1778-1809. https://doi.org/10.1016/j.dt.2021.09.011

Dastjerdi, S., Akgöz, B. and Civalek, Ö. (2020), "On the effect of viscoelasticity on behavior of gyroscopes", *Int. J. Eng. Sci.*, **149**, 103236. https://doi.org/10.1016/j.ijengsci.2020.103236

Eringen, A.C. (1984), "Plane waves in nonlocal micropolar elasticity", *Int. J. Eng. Sci.*, **22**(8-10), 1113-1121.

Esen, I., Daikh, A.A. and Eltaher, M.A. (2021), "Dynamic response of nonlocal strain gradient FG nanobeam reinforced by carbon nanotubes under moving point load", *Eur. Phys. J. Plus*, **136**(4), 1-22. https://doi.org/10.1140/epjp/s13360-021-01419-7

Esmaeilzadeh, M., Golmakani, M.A., Kadkhodayan, M., Amoozgar, M. and Bodaghi, M. (2021), "Geometrically nonlinear thermo-mechanical analysis of graphene-reinforced moving polymer nanoplates", *Adv. Nano Res.*, **10**(2), 151-163. http://doi.org/10.12989/anr.2021.10.2.151

Ghannadpour, S.A.M. and Moradi, F. (2020), "Nonlocal nonlinear analysis of nano-graphene sheets under compression using semi-Galerkin technique", *Adv. Nano Res.*, **7**(5), 311-324. http://doi.org/10.12989/anr.2019.7.5.311

Ghazwani, M.H., Alnujaie, A., Eltaher, M.A. and Van Vinh, P. (2024), "The role of nonlocality on low and high frequency behaviors of functionally graded sandwich nanoplates", *ZAMM-J. Appl. Math. Mech.*, e202400088. https://doi.org/10.1002/zamm.202400088

Gholami, R. and Ansari, R. (2019), "Nonlinear stability and vibration of pre/post-buckled multilayer FG-GPLRPC rectangular plates", *Appl. Math. Modell.*, **65**, 627-660. https://doi.org/10.1016/j.apm.2018.08.038

Guerroudj, M., Drai, A., Daikh, A.A., Houari, M.S.A., Aour, B., Eltaher, M.A. and Belarbi, M.O. (2024), "Size-dependent free vibration analysis of multidirectional functionally graded nanobeams via a nonlocal strain gradient theory", *J. Eng. Math.*, **146**(1), 20. https://doi.org/10.1007/s10665-024-10373-z

Hasrati, E., Ansari, R. and Torabi, J. (2017), "Nonlinear forced vibration analysis of FG-CNTRC cylindrical shells under thermal loading using a numerical strategy", *Int. J. Appl. Mech.*, **9**(8), 1750108. https://doi.org/10.1142/S1758825117501083

Jalaei, M.H. and Civalek, Ö. (2019), "On dynamic instability of magnetically embedded viscoelastic porous FG nanobeam", *Int. J. Eng. Sci.*, **143**, 14-32. https://doi.org/10.1016/j.ijengsci.2019.06.013

Kutlu, H. and Omurtag, H.M. (2012), "Large deflection bending analysis of elliptic plates on orthotropic elastic foundations using a mixed finite element method", *Int. J. Mech. Sci.*, **65**, 64-74. http://doi.org/10.1016/j.ijmecsci.2012.09.004

Li, Y.P. and She, G.L. (2024), "Nonlinear transient response analysis of rotating carbon nanotube reinforced composite cylindrical shells with initial geometrical imperfection", *Arch. Civil Mech. Eng.*, **24**(3), 161. https://doi.org/10.1007/s43452-024-00973-y

Lim, C., Zhang, G. and Reddy, J. (2015), "A higher-order nonlocal elasticity and strain gradient theory and its applications in wave propagation", *J. Mech. Phys. Solids*, **78**, 298-313. https://doi.org/10.1016/j.jmps.2015.02.001

Mehrez, S., Karati, S.A., DolatAbadi, P.T., Shah, S.N.R., Azam, S., Khorami, M. and Assilzadeh, H. (2020), "Nonlocal dynamic modeling of mass sensors consisting of graphene sheets based on strain gradient theory", *Adv. Nano Res.*, **9**(4), 221-235. http://doi.org/10.12989/anr.2020.9.4.221

Mercan, K., Demir, Ç. and Civalek, Ö. (2016), "Vibration analysis of FG cylindrical shells with power-law index using discrete singular convolution technique", *Curved Layered Struct.*, **3**(1). https://doi.org/10.1515/cls-2016-0007

Ninh, D.G., Ha, N.H., Long, N.T., Tan, N.C., Tien, N.D. and Dao, D.V. (2023), "Thermal vibrations of complex-generatrix shells made of sandwich CNTRC sheets on both sides and open/closed cellular functionally graded porous core", *Thin Wall. Struct.*, **182**, 110161. https://doi.org/10.1016/j.tws.2022.110161

Phon, N.D., Doan, T.N., Van Quang, D. and Van Minh, P. (2024), "Thermoelastic analysis of FG-CNTRC cylindrical shells with various boundary conditions and temperature-dependent characteristics using quasi-3D higher-order shear deformation theory", *J. Thermoplast. Compos. Mater.*, 08927057241274332. https://doi.org/10.1177/08927057241274332

Qu, Y., Jin, F. and Zhang, G. (2021), "Mechanically induced electric and magnetic fields in the bending and symmetric-shear deformations of a microstructure-dependent FG-MEE composite beam", *Compos. Struct.*, **278**, 114554. https://doi.org/10.1016/j.compstruct.2021.114554

Safaei, B., Khoda, F.H. and Fattahi, A.M. (2019), "Non-classical plate model for single-layered graphene sheet for axial buckling", *Adv. Nano Res.*, **7**(4), 265-275. http://doi.org/10.12989/anr.2019.7.4.265

Saffari, P.R., Ismail, S.O., Thongchom, C., Sirimontree, S. and Jearsiripongkul, T. (2024), "Effect of magnetic field on vibration of electrorheological fluid nanoplates with FG-CNTRC layers", *J. Vib. Eng. Technol.*, **12**(3), 3335-3354. https://doi.org/10.1007/s42417-023-01048-7

Shariati, A., Barati, M.R., Ebrahimi, F., Singhal, A. and Toghroli, A. (2020), "Investigating vibrational behavior of graphene sheets under linearly varying in-plane bending load based on the nonlocal strain gradient theory", *Adv. Nano Res.*, 8(4), 265-276. http://doi.org/10.12989/anr.2020.8.4.265

Shen, H.S. (2011), "Postbuckling of nanotube-reinforced composite cylindrical shells in thermal environments, Part I: Axially-loaded shells", *Compos. Struct.*, **93**(8), 2096-2108. https://doi.org/10.1016/j.compstruct.2011.02.011

Shen, H.S. and Zhang, C.L. (2010), "Thermal buckling and postbuckling behavior of functionally graded carbon nanotube-reinforced composite plates", Mater. Des., **31**(7), 3403-3411. https://doi.org/10.1016/j.matdes.2010.01.048

Shen, H.S., Li, C. and Huang, X.H. (2023), "Assessment of negative Poisson's ratio effect on the postbuckling of pressure-loaded FG-CNTRC laminated cylindrical shells", *Mech. Based Des. Struct.*, **51**(4), 1856-1880. https://doi.org/10.1080/15397734.2021.1880934

Shen, H.S., Li, C. and Reddy, J. (2020), "Large amplitude vibration of FG-CNTRC laminated cylindrical shells with negative Poisson's ratio", *Comput. Meth. Appl. Mech. Eng.*, **360**, 112727. https://doi.org/10.1016/j.cma.2019.112727

Sun, S., Guo, C., Feng, W. and Cao, D. (2022), "Nonlinear vibration analysis of CNT-reinforced functionally graded composite cylindrical shells resting on elastic foundations", *Int. J. Non-Linear Mech.*, **143**, 104037. https://doi.org/10.1016/j.ijnonlinmec.2022.104037

Thai, C.H., Ferreira, A.J.M., Tran, T.D. and Phung-Van, P. (2020), "A size-dependent quasi-3D isogeometric model for functionally graded graphene platelet-reinforced composite microplates based on the modified couple stress theory", *Compos. Struct.*, **234**, 111695. https://doi.org/10.1016/j.compstruct.2019.111695

Thai, H.T., Nguyen, T.K., Vo, T.P. and Lee, J. (2014), "Analysis of functionally graded sandwich plates using a new first-order shear deformation theory", *Eur. J. Mech. A Solids*, **45**, 211-225. https://doi.org/10.1016/j.euromechsol.2013.12.008

Thang, P.T., Thoi, T.N. and Lee, J. (2019), "Closed-form solution for nonlinear buckling analysis of FG-CNTRC cylindrical shells with initial geometric imperfections", *Eur. J. Mech. A Solids*, **73**, 483-491. https://doi.org/10.1016/j.euromechsol.2018.10.008

Tharwan, M.Y., Daikh, A.A., Assie, A.E., Alnujaie, A. and Eltaher, M.A. (2024), "Refined quasi-3D shear deformation theory for buckling analysis of functionally graded curved nanobeams on Winkler/Pasternak/Kerr foundations", *Mech. Based Des. Struct.*, **52**(9), 6101-6124. https://doi.org/10.1080/15397734.2023.2270043

Uzun, B. and Yaylı, M.Ö. (2024), "Accurate and efficient analytical simulation of free vibration for embedded nonlocal CNTRC beams with general boundary conditions", *Physica B*,

416139. https://doi.org/10.1016/j.physb.2024.416139
Vu, H.N., Do, T.K.M., Vu, M.D., Vu, T.H., Pham, T.H. and Nguyen, T.P. (2023), "A new analytical approach for nonlinear buckling and postbuckling of torsion-loaded FG-CNTRC sandwich toroidal shell segments with corrugated core in thermal environments", *Mech. Adv. Mater. Struct.*, 1-12. https://doi.org/10.1080/15376494.2023.2249458
Wang, S., Hong, J., Wei, D. and Zhang, G. (2023), "Bending and wave propagation analysis of axially functionally graded beams based on a reformulated strain gradient elasticity theory", *Appl. Math. Mech.*, **44**(10), 1803-1820. https://doi.org/10.1007/s10483-023-3042-6
Wang, S., Hong, J., Yin, S. and Zhang, G. (2024), "Isogeometric analysis of magneto-electro-elastic functionally graded Mindlin microplates", *Thin Wall. Struct.*, **198**, 111740. https://doi.org/10.1016/j.tws.2024.111740
Wu, H., Yang, J. and Kitipornchai, S. (2018), "Parametric instability of thermo-mechanically loaded functionally graded graphene reinforced nanocomposite plates", *Int. J. Mech. Sci.*, **135**, 431-440. https://doi.org/10.1016/j.ijmecsci.2017.11.039
Zhang, F. and Lu, W. (2024), "Non-linear free and forced vibration of bi-directional functionally graded truncated conical tube based on the nonlocal gradient strain theory", *Waves Random Complex Med.*, **34**(4), 2366-2393. https://doi.org/10.1080/17455030.2021.1956016
Zhao, L.C., Xu, L. and Zeng, H.T. (2024), "Thermal buckling of temperature-dependent FG-CNT reinforced composite conical-conical joined shell using GDQ", *Thin Wall. Struct.*, **205**, 112320. https://doi.org/10.1016/j.tws.2024.112320

CC